



Polypropylene Filled With Glass Spheres in Extrusion-Based Additive Manufacturing: Effect of Filler Size and Printing Chamber Temperature

Martin Spoerk,* Florian Arbeiter, Ivan Raguž, Georg Weingrill, Thomas Fischinger, Gerhard Traxler, Stephan Schuschnigg, Ludwig Cardon, and Clemens Holzer

A challenge in extrusion-based additive manufacturing of polypropylene (PP) filled with spherical particles is the combination of decent processability, excellent warpage control, and the retention of the tensile strength of neat PP. This study addresses this issue by adopting two approaches. Firstly, different size fractions of borosilicate glass spheres incorporated into PP are compared. Secondly, the temperature of the printing chamber (T_{Ch}) is varied. The effects of these features on the thermal, crystalline, morphological, tensile, impact, and warpage properties of 3D-printed parts are examined. Smaller glass spheres ($<12\ \mu\text{m}$) are found to be superior to larger fractions in all investigated aspects. Notably, the corresponding composites show higher tensile strengths than neat PP. An increase in T_{Ch} results in a more homogeneous temperature distribution within the printing chamber and promotes annealing during printing. Consequently, the dimensional accuracy of printed parts is improved. Additionally, β -crystals and larger spherulites are formed at a higher T_{Ch} .

to a computer aided design (CAD)-defined contour, in which successive layers are stacked upon each other. Therefore, a flexible filament is continuously transported by two counter-rotating driving wheels through a liquefier and a moving nozzle until the desired part is shaped.^[4–6] This technique allows the rapid, flexible, and cost-effective fabrication of diverse customized products.^[5] However, the range of commercially available materials that are flawlessly processable by means of FFF is still small.^[7] Although plenty of composites have been investigated,^[8] the base materials are still limited to a handful of polymer types. In particular, the FFF market lacks polymers for demanding technical applications. Polypropylene (PP), for example, is a promising material for FFF due to its high impact strength, chemical resist-


1. Introduction

Extrusion-based additive manufacturing, also known as material extrusion,^[1] fused filament fabrication (FFF), fused deposition modeling, or 3D printing, enables the mold-free fabrication of complex customized parts, which are hardly processable by any other conventional manufacturing method.^[2,3] The process relies on the selective deposition of thermoplastic strands according

ance, moisture stability, and low cost.^[9] However, little research has been conducted on the main drawback connected with the 3D printing of PP, which is the fact that PP parts are prone to dimensional inaccuracies, in particular to warpage.^[7,10–13] These are facilitated by the introduction of orientations during printing^[10] and the material's high crystallinity.^[14] The incorporation of low aspect ratio fillers improved this issue by successfully decreasing the warpage of 3D-printed PP parts.^[10] However, the

M. Spoerk, I. Raguž, S. Schuschnigg, Prof. C. Holzer
Polymer Processing
Montanuniversitaet Leoben
Otto Gloeckel-Straße 2, 8700 Leoben, Austria
E-mail: martin.spoerk@unileoben.ac.at

M. Spoerk, Prof. L. Cardon
Centre for Polymer and Material Technologies
Department of Materials
Textiles and Chemical Engineering
Ghent University
Technologiepark 915, 9052 Zwijnaarde, Belgium

 The ORCID identification number(s) for the author(s) of this article can be found under <https://doi.org/10.1002/mame.201800179>.

© 2018 The Authors. Published by WILEY-VCH Verlag GmbH & Co. KGaA, Weinheim. This is an open access article under the terms of the Creative Commons Attribution License, which permits use, distribution and reproduction in any medium, provided the original work is properly cited.

DOI: 10.1002/mame.201800179

Dr. F. Arbeiter
Materials Science and Testing of Polymers
Montanuniversitaet Leoben
Otto Gloeckel-Straße 2, 8700 Leoben, Austria
G. Weingrill
Mineral Processing
Montanuniversitaet Leoben
Franz-Josef-Straße 18, 8700 Leoben, Austria
Dr. T. Fischinger
Functional Surfaces and Nanostructures
Profactor GmbH
Im Stadtgut A2, 4407 Steyr-Gleink, Austria
G. Traxler
Machine Vision
Profactor GmbH
Graumanngasse 7, C3, 1150 Wien, Austria

fillers simultaneously deteriorated the mechanical properties of the PP composite. Consequently, it is necessary to find a way to ensure a consistent warpage control as well as suitable and isotropic mechanical properties of printed PP compounds.

Firstly, an optimized filler–matrix interface is needed for improved mechanical properties. Preliminary work by the authors^[12,15] investigated this optimization process for PP filled with glass spheres for the use in FFF. The most promising compound containing 30 vol% of coated borosilicate glass spheres resulted in a decent printability, 80% of the yield stress of neat PP, and a strain at yield comparable to that of neat PP. However, the warpage of printed parts has not been studied in detail. One possible approach to further improve the yield stress and simultaneously optimize the warpage behavior of the most promising compound of ref. [12] is to use selected size fractions of the fillers. The effect of different filler sizes on the warpage and the mechanical properties has not yet been investigated for optimized 3D-printed PP composites in detail, although smaller fillers promise a better shrinkage and warpage reduction.^[10] For example, both injection-molded polyamide 6 filled with glass beads^[16] and polybutylterephthalat/polyethyleneterephthalat containing talc^[17] showed a trend toward reduced part deformations for higher filler amounts and smaller filler sizes. Moreover, the augmented specific surface area of smaller glass spheres should also lead for 3D-printed parts to improved tensile^[18,19] and impact strengths,^[20] as has been found for injection-molded PP compounds.

Apart from changes in the material composition, another possibility to prevent warpage and improve the strength of printed PP composites is an adaptation of the printing process itself. Due to the complex temperature conditions during printing,^[21,22] which result from the repeated rapid heating and cooling of the material by the moving nozzle, the material is exposed to a rather inhomogeneous temperature distribution. As a result, a controlled crystal growth is impeded and internal stresses occur, which can cause part deformations.^[14,23,24] By increasing the temperature in the surroundings of the printed part in the build chamber, henceforth referred to as the printing chamber temperature T_{Ch} , a more homogeneous temperature distribution is achieved within the build envelope.^[25,26] Consequently, a higher T_{Ch} is expected to result in a reduced amount of warpage, as proposed in the mathematical model of Wang et al.^[27] These authors found for acrylonitrile butadiene styrene that ideally the warp deformation of printed parts should be zero, when the set T_{Ch} is around the glass transition temperature. This finding may be valid for amorphous polymers, but is impractical for semicrystalline polymers with a glass transition temperature below 0 °C, such as PP.^[7,10,11] For PP, a heat treatment at higher T_{Ch} , i.e., above 60 °C, can significantly alter the morphology, the crystallinity, as well as the size and homogeneity of the crystalline regions.^[28–30] For example, Wang and Gardner^[31] found that additively manufactured PP can additionally form β -crystals when exposed to a high T_{Ch} . However, they neither studied in detail the size and homogeneity of the crystalline regions nor the warpage or mechanical properties of printed parts as a function of the T_{Ch} . Nonetheless, the warpage of printed PP parts should be improved at a high T_{Ch} , as PP tends to approach a thermodynamically more stable state after a heat treatment^[29] and the internal stresses inside the printed

component tend to be reduced.^[26] Changes in the crystalline properties induced by a higher T_{Ch} can also have a positive effect on the yield stress of PP.^[28] Moreover, a homogeneous temperature distribution at higher temperatures is known to enhance the diffusion between adjacent printed strands.^[32] As a consequence, the intralayer bond strength was reported to be increased for higher T_{Ch} .^[33] In conclusion, an increased T_{Ch} may be expected to have a positive impact on various aspects in the extrusion-based additive manufacturing of thermoplastics. However, concerning 3D-printed PP, or especially optimized PP compounds, its promising effect on the warpage or the mechanical properties has so far never been studied in a systematic manner.

The present work aims at closing this gap by thoroughly investigating the effect of two different T_{Ch} , namely 25 and 55 °C, on the thermal, optical, mechanical, and warpage properties of 3D-printed parts made of neat PP and an optimized PP compound filled with 30 vol% borosilicate glass spheres. In order to additionally study the effect of the filler size, the composites are filled with borosilicate glass spheres of three size fractions (<12, 25–35, and 50–63 μm). The effects of both parameters on 3D-printed parts are simultaneously investigated, so that optimal material and processing parameters can be recommended.

2. Experimental Section

2.1. Materials

A polypropylene heterophasic copolymer (PP) with a melting temperature of 166 °C, a melt flow rate of 5 g per 10 min (230 °C, 2.16 kg), and a density of 0.905 g cm⁻³ was supplied by Borealis AG, Austria. All the glass spheres used in this work were solid borosilicate glass spheres (E-glass) in an aminosilane-coated condition obtained from Potters Europe, Germany. Based on the feed material Spheriglass 3000E, which exhibits a wide size distribution (please refer to ref. [12]), three filler fractions with comparable narrow size distributions and different mean filler diameters were produced by various sieving steps by means of a Haver EML 450 Digital Plus (Haver & Boecker OHG, Germany) test sieve shaker and appropriate sieves (Retsch GmbH, Germany). The particle size range for the fillers was smaller than 12 μm (E-1), between 25 and 35 μm (E-2), and between 50 and 63 μm (E-3), respectively. The exact particle size distribution, measured by dynamic light scattering with a Mastersizer 2000 (Malvern Instruments Ltd, UK), as well as the scanning electron microscopy (SEM) images of the three fillers are summarized in **Figure 1**. The compatibilizer SCONA TPPP 9212 GA (Comp.), based on PP functionalized with maleic anhydride, was supplied by BYK-Chemie GmbH, Germany. The amorphous polyolefin Aerafin 180 (am.PO) was supplied by Eastman Chemical Company, USA.

2.2. Preparation of Composites

All composites (**Table 1**) were processed by mixing the materials for 30 min at 200 °C in a lab kneader (Polylab Rheomix 3000, Thermo Fisher Scientific Inc., Germany) equipped with

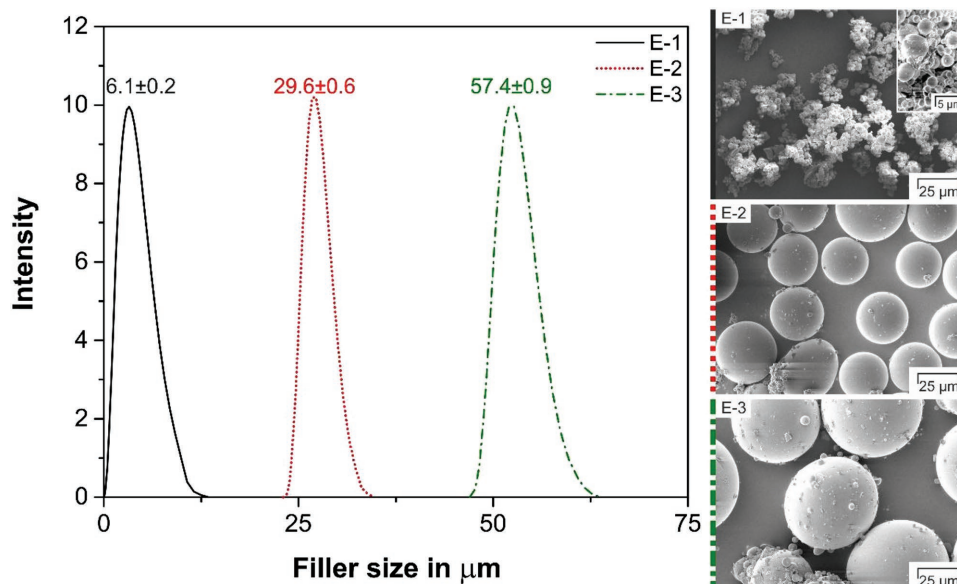


Figure 1. Normalized particle size distribution with the measured mean particle size values and the scanning electron microscopy images at a magnification of 2000× for the three fillers investigated. For filler E-1, a magnified image is added in the top right corner to give a better visualization of the shape of the fillers. On fillers E-2 and E-3, few very small particles from the feed material adhere to the main filler fraction due to interparticulate adhesion forces.^[34] As the amount of these small particles on fillers E-2 and E-3 is negligible they are not expected to influence the properties of the final composites.

two counter-rotating roller blades at a rotation of 60 rpm. A constant glass filler content of 30 vol% was investigated in order to reduce the warpage of the printed composites in a most promising manner.^[10,12] For all the filled compounds, PP was melted for 2 min. Subsequently, 6.8 vol% of am.PO was added and mixed to the fully melted polymer. After an additional 2 min, 2 vol% of the compatibilizer was included and everything was mixed for 4 min. Then, the glass fillers were added to the compound. After completing the kneading, the mixtures were removed in the melt state from the mixing chamber and cooled down to room temperature. The compounds were ground to pellets in a cutting mill (SM200, sieve with square perforations of 4 × 4 mm², Retsch GmbH, Germany) and stored under standardized conditions (23 °C air temperature, 50% relative humidity). One reference sample of neat PP was prepared under the same conditions as described above.

2.3. Preparation of Filaments

The ground materials were processed to filaments in the single screw extruder FT-E20T-MP-IS (Dr. Collin GmbH,

Table 1. Compositions and designations of the compounds consisting of polypropylene (PP), the amorphous polyolefin (am.PO), the compatibilizer (Comp.), and the different filler types.

Sample designation	PP [vol%]	am.PO [vol%]	Comp. [vol%]	Filler type	Filler [vol%]
PP	100.0	–	–	–	–
PP/E-1	61.2	6.8	2.0	E-1	30.0
PP/E-2	61.2	6.8	2.0	E-2	30.0
PP/E-3	61.2	6.8	2.0	E-3	30.0

Germany) using the following settings: screw speed = 30 rpm, heating zones of the extruder barrel = 175, 180, and 185 °C, die diameter = 1.9 mm, die length = 25.05 mm. The extrudate was pulled by a winding unit through a 3 m long water bath set to ≈50 °C. To comply with the diameter tolerances of the filaments of 1.75 ± 0.05 mm as well as a low ovality, the filaments' diameter data were recorded prior to spooling by a Sikora Laser 2010T diameter measurement device and the Ecocontrol 600 processor (Sikora AG, Germany). Before printing or subsequent characterization steps, the spooled filaments were stored under standardized conditions.

2.4. Morphology Analysis

The filler–matrix interaction as well as the filler distribution in the cryofractured filaments were investigated by means of SEM on a Tescan Vega II (Tescan Brno s.r.o., Czech Republic) at 5 kV using secondary electrons. Prior to the analysis, the specimens were mounted on a sample holder with a carbon tape and sputtered with gold for 100 s at 20 mA. Additionally, the sizes of the sieved fillers (Figure 1) were double-checked and the fracture surfaces of tested, printed Charpy specimens were analyzed by SEM with the same settings.

2.5. Preparation of Printed Specimens

All printed parts were produced by means of a Duplicator i3 v2 (Wanhao, China) FFF printer with a steel nozzle of 0.6 mm in diameter and sliced with the software Simplify3D Version 3.0 (Simplify3D, USA). The parameters summarized in Table 2 were used for all the specimens. The infill density of all the printed parts was adjusted depending on the material so that the cross-sections

Table 2. Values of the printing parameters of all printed specimens in this work.

Printing parameters	Value
Nozzle temperature [°C]	230
Printing bed material	PP plate
Printing bed temperature low; high [°C]	20; 70
Layer thickness [mm]	0.25
Printing speed of the first layer [mm s ⁻¹]	28.3
Printing speed of all the subsequent layers [mm s ⁻¹]	56.6
Flow rate of the first layer [percent of the flow rate of the subsequent layers]	150

of all printed specimens exhibited a minimal and comparable amount of air gaps. This was tested for each specimen type for neat PP and PP/E-1 prior to the actual specimen fabrication by means of optical microscopy (SZH, Olympus Optical Co.). For the other filled filaments, this was controlled by the mass of the printed specimens. As all the filled composites had the same volumetric filler concentration and the fillers obtained had the same density, the mass of each printed specimen was kept constant for PP/E-1, PP/E-2, and PP/E-3, respectively.

The PP printing plate was based on a heterophasic PP copolymer, which was chosen due to its slightly different polarity compared to that of the base PP of the filament. Hence, the risk of welding between the first printed layer and the printing bed was slightly decreased,^[35] but at ideal processing parameters, a decent amount of adhesion was still given. The plate of a size of 160 × 160 × 10 mm³ was produced by compression molding in a P200PV vacuum press (Dr. Collin GmbH, Germany) at 200 °C under 120 bar for 15 min. To evaluate the effect of the T_{Ch} , printing bed temperatures of 20 and 70 °C were used. Based on the former setting, a T_{Ch} of roughly 25 °C was reached. In the case of the latter setting, the whole printer was insulated with expanded polystyrene plates, so that a T_{Ch} of 55 °C was achieved. The temperature evolution and determination of the T_{Ch} are displayed in Figure S1 (Supporting Information). It showed that the higher T_{Ch} resulted in smaller temperature fluctuations and therefore in a more homogeneous temperature distribution within the build chamber. Prints at a T_{Ch} higher than 55 °C were not conducted in order to prevent failure of essential machine components such as the stepper motors. As soon as a constant T_{Ch} was reached, the build cycle was started. After its completion, the insulation was removed and the printing bed was cooled down to room temperature for ≈15 min. The manufactured specimens were detached from the build platform with a spatula and stored under standardized conditions for at least 72 h until subsequent tests were performed.

2.6. Thermography

The evolution of the T_{Ch} as well as the temperature of a fixed position in a Charpy specimen was recorded by thermography measurements. For the latter one, a fixed position on a contour strand in the third printing layer of the first of five Charpy specimens was monitored during the whole build cycle under

an angle of 1.8° in order to investigate the temperature of the printed strands themselves. Details on the test setup were represented next to the respective results for better visualization in Section 3.2.1. For all the tests, the thermal camera Silver450 (Cedip Infrared Systems, France) equipped with a lens of a focal length of 27 mm captured the temperature evolution between 25 and 103 °C at a sampling rate of 1 Hz and a local resolution of 340 μm per pixel. The distance between the camera and the measured Charpy specimen was constantly 0.2 m.

2.7. Thermal Analysis

The melting and crystallization behavior of the filaments as well as of the Charpy specimens printed at both T_{Ch} of all the materials were analyzed by means of differential scanning calorimetry (DSC). For the latter, pieces were cut from the center of a cross-section located roughly 20 mm off the edge of an untested Charpy specimen. Seven specimens per material and T_{Ch} , each having a mass of 10 ± 1 mg, were investigated in a DSC 1 equipped with a gas controller GC 200 (both Mettler Toledo GmbH, Switzerland) under a constant nitrogen flow of 50 mL min⁻¹. All the samples were exposed to heat-cool-heat runs between 25 and 200 °C with the heating and cooling rate set to 10 and 20 K min⁻¹, respectively. All the obtained values were evaluated to a significance level of 5%. For calculating the degree of crystallinity, the mass fraction of the filler was incorporated into the calculation, as described in ref. [36] and the heat of fusion of a fully crystalline PP was taken as 207 J g⁻¹.^[37]

2.8. X-Ray Diffraction (XRD) Measurements

XRD measurements were performed on a Bruker D8 Discover XRD system equipped with a Cu X-ray source ($\lambda = 1.5406 \text{ \AA}$) and a linear X-ray detector (all Bruker Corporation, USA). Samples with a thickness of 600 μm were cut from the center of a cross-section located roughly 20 mm off the edge of an untested Charpy specimen and were put on a silicon sample cup on the sample heating stage. θ - 2θ measurements between 5° and 55° were carried out in air at atmospheric pressure at room temperature in reflection mode. In order to measure the reference material without influences from the processing history, the samples were additionally tested after being heated from room temperature to 200 °C and cooled down to room temperature at the same heating/cooling rates as described in Section 2.7. The temperature was measured with a K-type thermocouple and during heating/cooling, the samples were subjected to a controlled Helium flow of 250 cm³ min⁻¹.

2.9. Polarized Optical Microscopy

To investigate the effect of the T_{Ch} on the spherulite size, slices of 20 μm, taken from the middle of an untested printed Charpy specimen and obtained by the Leica RM 2255 (Leica Microsystems GmbH, Germany) microtome, were analyzed in the polarized optical microscope Olympus SZX12 (Olympus Life Science Europe GmbH, Germany) under transmitted light.

2.10. Tensile Tests

Tensile tests were performed on the filament as well as on printed shortened tensile test specimens under standardized conditions. The former were tested on a Zwick Z001 (Zwick GmbH & Co. KG, Germany) with a 1 kN load cell, at a gauge length of 50 mm and a testing speed of 10 mm min⁻¹. All the tests of the latter were performed on the universal testing machine Zwick Z010 (Zwick GmbH & Co. KG, Germany) with a load cell of 10 kN, a gauge length of 40 mm, a preload of 0.1 MPa, and a testing speed of 1 mm min⁻¹ for the determination of the Young's modulus and 50 mm min⁻¹ until rupture. As the shortened tensile test specimens were printed with a strand orientation perpendicular to the loading direction (90° orientation), it was possible to characterize the influence of the filler and T_{Ch} on the interface between adjacent strands. All the results were evaluated to a significance level of 5%.

2.11. Charpy Tests

The Charpy specimens (80 × 10 × 4 mm³) were printed in a way that all the strands were oriented perpendicularly to the impact direction, resulting in a unidirectional orientation. With this setup, solely the influence of the glass fillers and the T_{Ch} on the impact properties could be measured. Per print, five specimens with a distance of 5 mm to each other were produced. Ten specimens (ISO 179-1 type 1/e/A) per material and T_{Ch} were notched by a wedge-shaped blade with a notch depth of 2 mm and a tip radius of 0.25 mm and tested in an edgewise direction in a randomized order according to standard ISO 179-1. The tests were performed on the impact testing pendulum Resil 25 (CEAST/Instron, Italy) at room temperature. The results were evaluated to a significance level of 5%.

2.12. Warpage Analysis

The effect of the filler distribution and the T_{Ch} on the warpage was characterized on printed parts that were especially prone to warpage on the corners, as exemplified by ref. [10]. In the present study, the thickness of the warpage specimen displayed in ref. [10] was doubled to 4 mm, while the printing orientation stayed the same. With this specimen, it was possible to visualize even small differences in warpage, as thicker parts show a trend toward higher part deformation and shrinkage.^[14] Prior to the warpage analysis, excess material on the surface of the printed warpage specimen was removed in order not to influence the subsequent warpage characterization. As heavily warped parts easily tilted over in their printing position after being removed from the printing bed, all the specimens were measured upside-down. In order to obtain a 2D representation of the actual shape of the printed parts, a point cloud was recorded at a working distance of 300 mm with a measurement duration of 2 s by means of the ShapeDrive SD-3 sensor (ShapeDrive GmbH, Germany). To compare the data acquired from the printed parts with the geometry in the CAD file, and, thus, to get a visual representation of the warpage

of the printed parts, the 3D point cloud and triangular mesh processing software CloudCompare version 2.6.1 by Daniel Girardeau-Montaut was used.

3. Results and Discussion

In order to verify whether all the materials are printable, only the filament properties were investigated in a first step. Later on, the properties of the printed materials were studied.

3.1. Filament Properties

3.1.1. Morphology

Prior to the investigations on printed parts, the morphology and the tensile tests of the filaments (**Figure 2**) were investigated in order to verify whether the FFF process requirements are met.^[12] The matrices of all the filled materials investigated (Figure 2b–d) exhibit a similar morphology compared to that of neat PP (Figure 2a). As the investigated composites of the present work are based on the optimized composition of ref. [12], all the composites show a homogeneous filler distribution, as highlighted for all fillers (Figure 2b–d) by white circles for reasons of clarity. This enables a constant printing flow rate over time and does not lead to blocked nozzles. Moreover, a good matrix–filler interface is observed for all the composites, since the fillers are not pulled out of the matrix, but are surrounded by it.^[38,39] The existence of larger parts torn out of the matrix, as can be seen in Figure 2c, can be referred to the added am.PO encapsulating the filler, which is known for such compositions and discussed in detail in previous works.^[10,12]

3.1.2. Filament Tensile Tests

In terms of mechanical properties, the requirements that need to be discussed for a successful use of the filament material in FFF are the Young's modulus E_t , the yield stress σ_Y (equaling the ultimate tensile strength for the filled materials) and the corresponding strain ε_Y (equaling the elongation at break for the filled materials).^[10,12] These values for the materials investigated are summarized in Table S1 (Supporting Information). The corresponding stress–strain curves are depicted in Figure 2e. It is known from previous works^[12] that the Young's modulus for PP compounds is not the limiting factor for FFF. Moreover, the modulus measured on the filaments can vary heavily, as the slight filament curvature can cause instabilities at the beginning of the loading regime. Hence, the following discussion focuses on trends relating to σ_Y and ε_Y . As the polymer chain mobility is decreased due to the addition of the rigid microspheres,^[40] the elongation at break of the composites is decreased sharply compared to that of neat PP and the ε_Y is reduced by roughly 30–60%. These latter differences in ε_Y between the composites, as well as their changes in σ_Y can be mainly referred to the filler size, as all the compounds exhibit a good filler–matrix

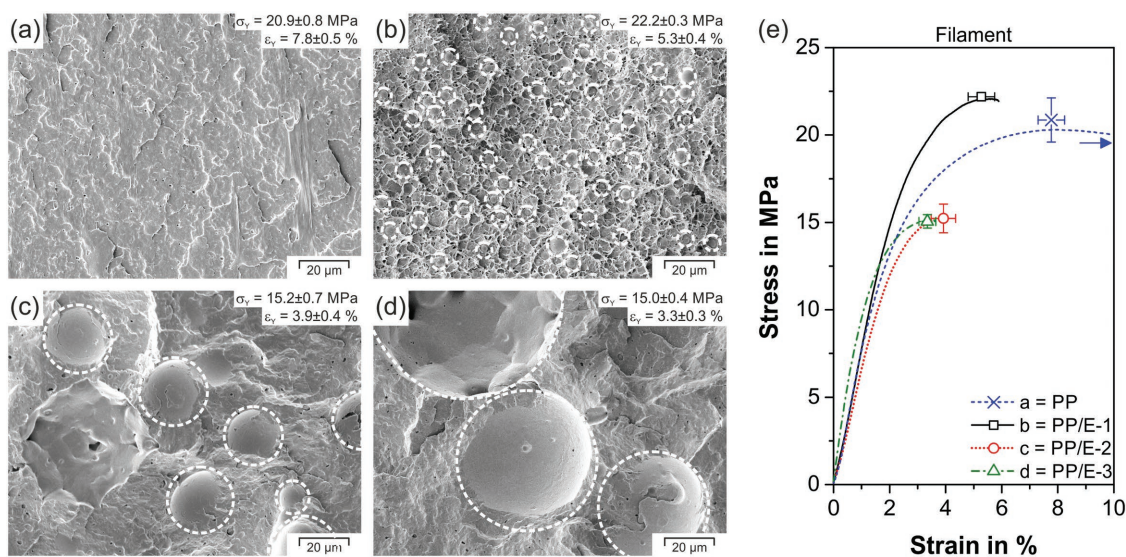


Figure 2. Scanning electron microscopy images of the cryofractured filaments of a) the neat PP and the compounds b) PP/E-1, c) PP/E-2, and d) PP/E-3 and e) the representative stress–strain curves of the four materials measured directly from the filaments. In the top right corner of each image of (a)–(d), the corresponding mean and 95%-confidence interval of the measured yield stresses σ_Y and elongations at yield ϵ_Y are shown. In (b)–(d), the fillers are highlighted with white circles to visualize their distribution. In (e), the mean and confidence interval for a significance level of 5% for the yield stress and the corresponding strain are marked by symbols and error bars. Although the neat PP filament exhibits a strain at break of $1631 \pm 21\%$ [marked by the arrow in (e)], only the first 10% of strain is represented for reasons of clarity.

interface and an even filler distribution (Figure 2b–d). Among the composites, the one containing the smallest fillers (PP/E-1) has both the highest σ_Y (22.2 ± 0.3 MPa) and ϵ_Y ($5.3 \pm 0.4\%$), because of the smaller flaw sizes induced by the smaller fillers.^[41] PP/E-1 even has a significantly higher σ_Y than neat PP (20.9 ± 0.8 MPa), despite the known stress-reducing effect of the am.PO in PP.^[10,12,42] The insignificantly different mechanical properties in compounds PP/E-2 and PP/E-3 show, compared to PP/E-1, a drop in σ_Y and ϵ_Y of $\approx 30\%$, respectively. This decrease may be explained by the thickness of the am.PO encapsulation around the glass spheres.^[43] Due to the smaller specific surface area of the larger spheres in PP/E-2 and PP/E-3 at the given 30 vol% filling, the am.PO encapsulation may be thicker than in PP/E-1. This may alter the constraint effect of the filler,^[41] resulting in lower σ_Y and ϵ_Y . In ref. [12], a similar decrease in σ_Y (roughly 20%) is observed for the same PP compound filled with the broadly distributed glass spheres Spheriglass 3000E (0–80 μm), which is the base material classified into the three filler fractions in the present work (Section 2.1). This decrease is less pronounced, as all the filler fractions are included. All in all, the composites investigated in the present work satisfy the filament requirements for the use in FFF, both in terms of mechanical and morphological properties.^[12]

3.2. Properties of the Printed Parts

3.2.1. Thermography Measurements

To fully understand the properties of the printed parts, in particular the influence of the different T_{Ch} , in situ

thermography measurements on neat PP were conducted during printing of the Charpy specimens for both T_{Ch} . These measurements (Figure 3a) show that a contour strand in a Charpy specimen can experience strand temperatures considerably higher than the set T_{Ch} . For both T_{Ch} , the minimum strand temperature as well as the mean strand temperature T_{mean} increase by roughly 22 and 30 °C, respectively, due to the adjacent, recently deposited, and therefore warmer strands and the close proximity of the nozzle (230 °C). Temperature peaks occur repeatedly, when the hot nozzle deposits strands on the specimen, on which the temperature is measured in the measurement position (Figure 3b). Due to the printing sequence (Figure 3b), one peak represents two subsequent layers that are printed directly after each other. Similar to ref. [25], the peak maxima decrease over time, as the subsequently deposited layers act as a thermal barrier for the measurement position. Due to the set temperature range of the thermal camera between 25 and 103 °C (Section 2.6), the measured temperatures for the T_{Ch} of 55 °C that were above 103 °C were cut off, because the sensor was saturated prior to reaching the maximal temperature. Therefore, the peak temperatures are expected to be higher than those presented in Figure 3. Hence, also the T_{mean} for a T_{Ch} of 55 °C could actually be slightly higher than 84.4 °C (Figure 3a). It should be mentioned that these measured temperatures should serve as guiding values to understand the morphology and crystalline properties of the material, and that they are only valid for this one measurement position. For example, a contour strand of a Charpy specimen that is surrounded on both sides by other specimens, or even a strand that is located in the center of the specimen, would result in further augmented T_{mean} due to the proximity of additional heat sources.^[44]

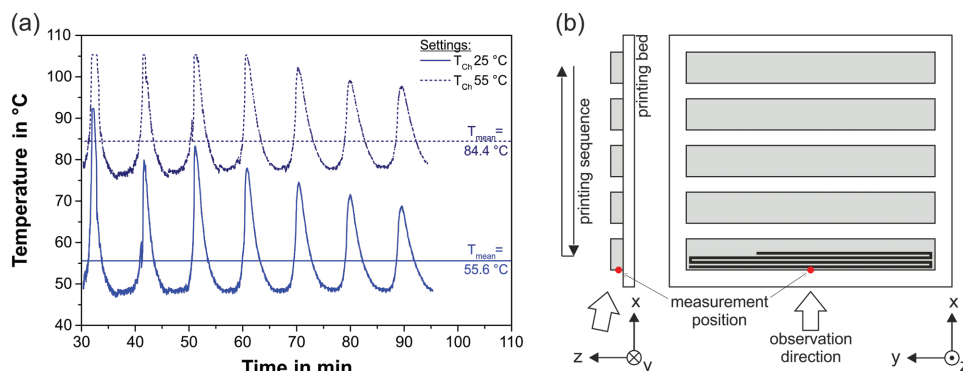


Figure 3. a) The temperature evolution of the contour strand of the third printing layer of the first Charpy specimen for both chamber temperatures T_{Ch} and b) a sketch of the experimental setup of the thermography measurements. In (a), the mean temperatures of the strand in the third layer (T_{mean}), calculated between the deposition of the investigated strand (at 30 min) and the completion of the print (at 95 min) are marked as horizontal lines for both T_{Ch} . In (b), the gray rectangles represent the Charpy specimens and the white one the printing bed. The measurement position, printing sequence, and observation direction are highlighted by red points and arrows, respectively. The coordinate system represents the part orientation in (b).

3.2.2. Thermal Properties

To understand the thermal behavior of the investigated materials and the influence of the processing conditions, the crystallization temperature T_{Cryst} , the degree of crystallinity α_{Cryst} and the melting behavior, in particular the melting peak temperature T_{Melt} were studied on the filaments and on untested Charpy specimens printed at a T_{Ch} of 25 and 55 °C (Table S2, Supporting Information). **Figure 4** displays the T_{Cryst} for all the materials as a function of processing conditions. Compared to neat PP ($T_{Cryst} = 111.4 \pm 0.7$ °C), all the filled filaments exhibit considerably increased T_{Cryst} because glass spheres are known to nucleate PP.^[12,45,46] The compound containing the smallest filler (PP/E-1) seems to nucleate the PP matrix in the most efficient way. Compared to neat PP, an increase of roughly 12% to 125.3 ± 0.9 °C is observed. The compounds PP/E-2 and PP/E-3, though, show a similar T_{Cryst} (116.8 ± 0.6 and 118.9 ± 0.5 °C, respectively) that is in between that of PP/E-1 and neat PP. The

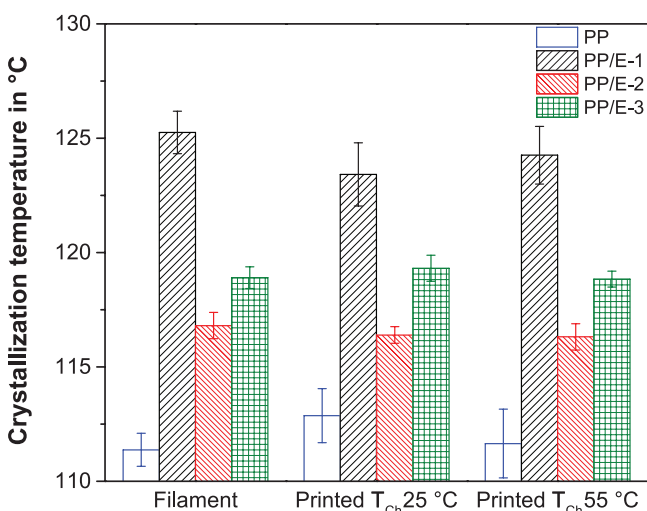


Figure 4. Crystallization temperature of neat PP and the three investigated composites measured on the filament or from parts printed at a chamber temperature T_{Ch} of 25 and 55 °C.

main reason for this trend is the larger specific surface area of smaller particles, resulting in a higher nucleation activity, as reported for other spherical fillers such as inorganic soda lime glass,^[47] perlite,^[10] or silica.^[48] The investigations on the printed Charpy specimens show the same trends for the T_{Cryst} as the filaments, independent of the T_{Ch} . The additional processing step does not seem to have an influence on the crystallization temperature of the material, as no significant differences compared to the filaments were observed.

The α_{Cryst} , which should be low for a decent printability and dimensional control,^[12] shows a slight, but not always, significant decrease for the filled materials compared to that of neat PP (Table S2, Supporting Information). This trend is expected, since 10 vol% of semicrystalline PP is replaced by the am.PO, and is in accordance with the literature.^[12,49] Among the composites, no significant difference in α_{Cryst} is observed, similar to ref. [10]. As a result, the constant α_{Cryst} in the present work most likely neither influences the tensile test results (Sections 3.1 and 3.2.4) nor the warpage analysis (Section 3.2.6), which both depend on the α_{Cryst} .^[14,23]

As the trends for the T_{Melt} do not show a comprehensible trend in Table S2 (Supporting Information), the melting curves are summarized for all the materials and processing steps in **Figure 5**. In order to see a direct influence of the T_{Ch} , the first heating cycles are compared. All the filled filaments exhibit a decrease in T_{Melt} compared to neat PP, most certainly due to the am.PO, which is known to change the melting behavior of PP.^[12,49–52] Additionally, a transcrystallization or a reorganization of crystals induced by the fillers could have reduced the T_{Melt} ^[53,54] and increased the melting onset temperature compared to neat PP.^[48] The filler size does not seem to have a significant impact on the melting behavior, as the melting peaks of all the three composites nearly overlap (Figure 5). As the strand temperatures observed during printing of the Charpy specimens printed at a T_{Ch} of 25 °C were clearly below 100 °C (Figure 3), which is the starting temperature for the formation of other crystal modifications,^[47] the melting curves of the first heating cycle appear similar to those of the filaments. At a first glance, the melting behavior of neat PP and PP/E-1 seems to be marginally altered by showing a broader peak slightly

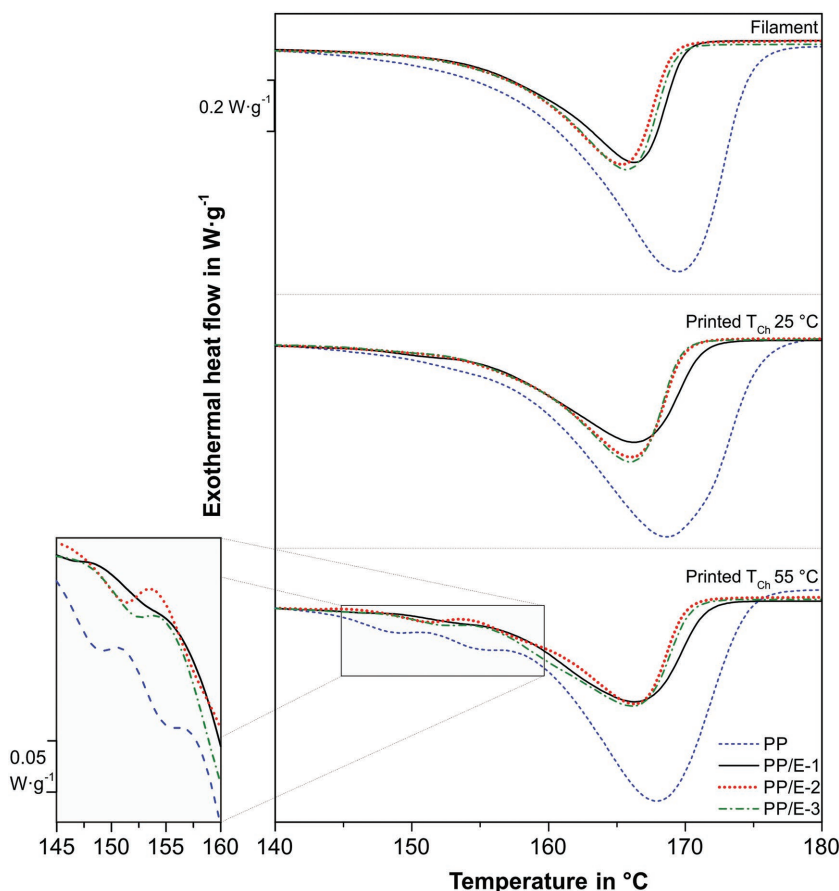


Figure 5. The DSC melting thermograms obtained from the first heating cycle for all the materials investigated. The results are presented for the filament and the untested Charpy specimens printed at a chamber temperature T_{Ch} of 25 and 55 °C. On the bottom left, a magnified image between 145 and 160 °C is displayed for a better visualization of the additional melting peaks occurring at a T_{Ch} of 55 °C.

shifted to higher temperatures. However, these trends are not significant and could therefore be introduced by minor differences in the sample preparation.^[55] An increase in the T_{Ch} to 55 °C, though, seems to significantly change the melting behavior of all the investigated materials, as additional melting peaks or shoulders between 145 and 160 °C (magnification in Figure 5) occur. Since the crystal modification depends on the cooling history,^[56] this finding can be caused by the relatively long exposure time of the material to temperatures between 75 and 105 °C during printing (Figure 3). The printing time for five Charpy specimens equals 95 min. This time may be long enough to already start some annealing processes in the matrix,^[28] which can alter the crystallization behavior.^[14] Annealing temperatures between 105 and 140 °C,^[57] such as measured on the strands in the present work (Figure 3), facilitate the growth of β -crystals.^[58] This is especially true for temperatures near the lower temperature limit.^[47] According to studies on PP filled with inorganic soda lime glass spheres,^[47,59] β -crystals melt around 147 °C, which roughly corresponds to the observed peak and shoulder temperatures between 146 and 151 °C for all the investigated materials (magnification in Figure 5). The additional peak at 154 °C,

which is only observed for neat PP, can be referred to the melting of β -crystals, which most likely formed in a recrystallization step during the heating cycle of the DSC.^[31,60] In addition to the temperature effect, the growth of β -crystals can be promoted by the induced orientations^[61] and high shear rates,^[62,63] both present during extrusion-based additive manufacturing.^[3,64,65] A similar β -crystallization has been observed for 3D-printed neat PP at a rather high T_{Ch} of 130 °C and a nozzle temperature of 200 °C.^[31] In contrast to this study, the present work shows that a combination of the considerably lower T_{Ch} of 55 °C, which is feasible on standard FFF printers, with a higher nozzle temperature of 230 °C is sufficient for the formation of β -crystals in addition to α -crystals.

In order to verify the additional peaks of the first DSC heating curve for a T_{Ch} of 55 °C (Figure 5), the diffraction pattern of neat PP printed at a T_{Ch} of 55 °C is plotted in Figure 6. Additionally, the room temperature diffraction pattern of the same material after the controlled heat-cool cycle is shown. It reflects the crystal structure of the PP without any processing influences and serves in the following as a reference. Its pattern reveals peaks at 14.1°, 16.9°, 18.5°, 21.1°, and 21.7°, corresponding to the (110), (040), (130), (111) and (131) and (041) reflections of the monoclinic α -crystal.^[66] The specimen that is measured after printing at a T_{Ch} of 55 °C (Figure 6) exhibits essentially the same peaks. However, in addition, one extra peak at 16.1° and one

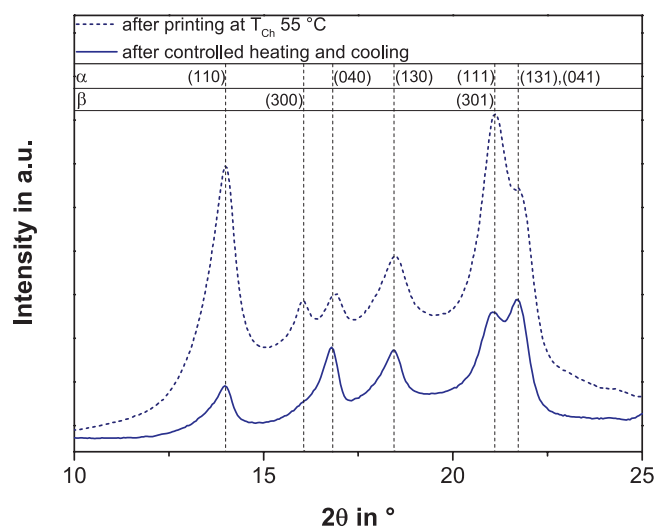


Figure 6. X-ray diffraction patterns for neat PP printed at a chamber temperature T_{Ch} of 55 °C. Both the measurements were conducted at room temperature; one before and one after the controlled heat-cool cycle. All the major peaks are indexed and attributed to α - or β -crystals.

intensified peak at 21.1°, corresponding to the (300) and (301) plane of hexagonal β -crystals, are found.^[66] As expected from the DSC (Figure 5) and the thermography measurements (Section 3.2.1), the annealing at the higher T_{Ch} results in a mixture of α - and β -crystals in neat PP, similar to refs. [31,58,63,66].

The relative intensities of reflections (110), (040), and (130) are different for the measurements before and after the heat-cool cycle. This can be explained by the flow-induced orientations of the spherulites (see Section 3.2.3) that originate from the FFF process.^[65,67] After the melting and controlled cooling step, the processing texture and morphology are largely deleted. During cooling, only a weak texture is developed. The difference in the overall intensities relates to differences in the probed sample volume. After melting, the material can spread on the sample holder. Therefore, the sample thickness decreases, resulting in a smaller diffracting volume. Consequently, the overall intensity level appears decreased.

3.2.3. Polarized Optical Microscopy

It is known for poly(lactic acid) (PLA) that in extrusion-based additive manufacturing, smaller crystals are more prominent than enlarged ones, as the frequent temperature fluctuations during printing (Figure 3) can form more nucleation points.^[32] Moreover, it is expected that these formations of nucleation events dominate the crystal growth, so that changes in the T_{Ch} can only influence the crystal size

to a small extent.^[32] In order to probe the validity of these findings for neat PP, polarized optical microscopy images are shown for the two T_{Ch} in Figure 7. At a first glance, no big differences between the Charpy specimens printed at a T_{Ch} of 25 °C (Figure 7a) and 55 °C (Figure 7b) can be discerned. Only the weld lines between adjacent strands appear pronounced for both the processing temperatures, as they exhibit considerably smaller crystal structures in the interface, similar to 3D-printed PLA^[32] or vibration-welded PP.^[68] When having a closer look to the strands (Figure 7c,d), though, a clear spherulite size difference is observed for the two T_{Ch} . The specimen printed at a T_{Ch} of 55 °C (Figure 7d), which partly contains β -crystals (Figures 5 and 6) that normally tend to form smaller spherulites for PP,^[69–71] exhibits spherulites that are approximately double the size ($\approx 50 \mu\text{m}$) than those printed at a T_{Ch} of 25 °C (Figure 7c, $\approx 25 \mu\text{m}$). This finding relates to the different crystal growth and nucleation rates at the two temperatures. The part printed at a T_{Ch} of 55 °C, in which the strands have a T_{mean} of 84.4 °C (Figure 3) for at least 95 min, shows a high crystal growth rate and a low nucleation rate, as the T_{mean} is close to the temperature of the maximum crystal growth rate, which is at 77 °C for PP.^[23] Hence, few nuclei grow at a rather high rate, resulting in large spherulites (Figure 7d), which is in accordance with studies on annealed PP.^[72] For the part printed at a T_{Ch} of 25 °C, the crystal growth rate is considerably lower than that of the specimen printed at a T_{Ch} of 55 °C, as the T_{mean} of 55.6 °C (Figure 3) is lower than the maximum crystal growth

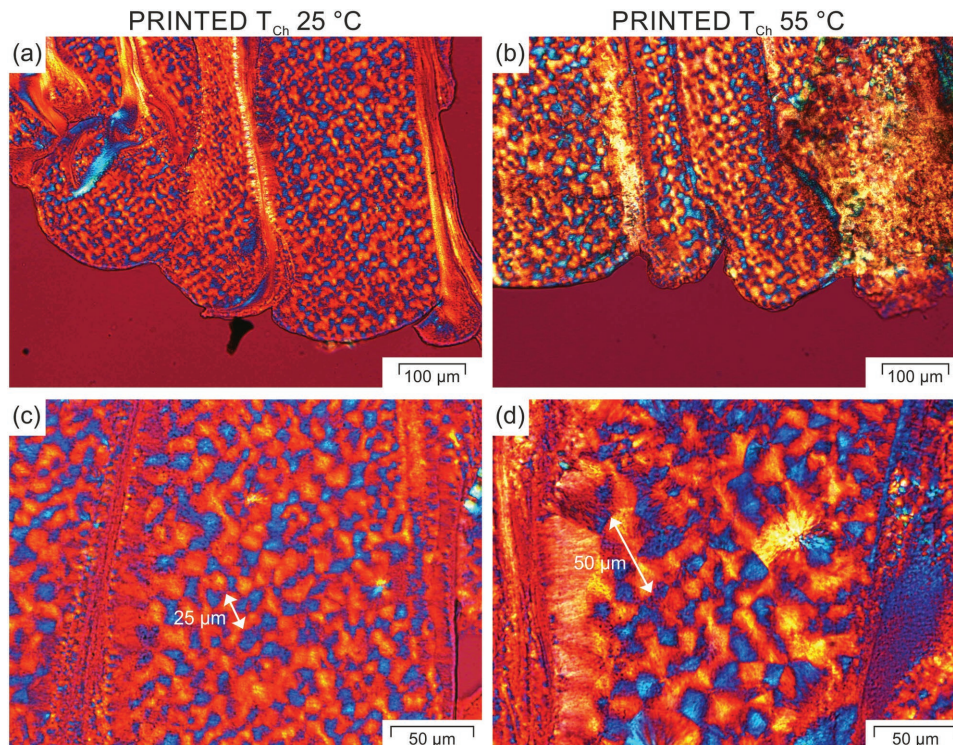


Figure 7. Polarized optical microscopy images of microtome cuts of untested Charpy specimens made of neat PP printed at a chamber temperature T_{Ch} of a,c) 25 °C and b,d) 55 °C, in which the longitudinal strands of one layer are visible. The overview images (a,b) represent deposited strands and their interdiffusion zones. The zoom images (c,d) exemplify the difference in spherulite size. The approximate diameter of one spherulite is exemplarily highlighted by white arrows in (c) and (d).

rate of 77 °C. Thus, the nucleation rate is higher,^[23] resulting in more nuclei that grow at a lower rate. Consequently, the spherulites are small but numerous (Figure 7c). To sum up, for printing/annealing times of 95 min, an increased T_{Ch} strongly influences the crystal size of neat PP, in contrast to the expectations of ref. [32]. Moreover, in contrast to Figure 7c, some of the spherulites shown in Figure 7d likely show the β -modification, as a comparison to those studied in the literature suggests.^[73]

Due to the flow-induced orientation of the polymer during printing, an orientation-induced crystallization occurs in parts of the strands in the shape of shish-kebab structures, similar to ref. [61]. An exemplified representation of such shish-kebab structures is displayed in Figure S2 (Supporting Information). The existence of these structures also confirms the relative intensity differences in the XRD measurements due to the flow-induced orientations (Figure 6).

Due to the heterogeneous nucleation of the crystals on the glass fillers (Figure 4), the amount of nuclei in the composites may have increased compared to neat PP, which may have resulted in smaller spherulites.^[74,75] Hence, similar polarized optical microscopy investigations on the filled materials would offer insights into their crystal growth. However, the necessary thickness of the microtome cut of 20 μm limits the application of this technique to the composite containing the smallest glass spheres (PP/E-1), as the larger fillers destroy the morphology during cutting. For the composite PP/E-1, the high amount of small fillers hampers the transmittance of the light, as can be seen on the polarized optical microscopy images in Figure S3 (Supporting Information). As a result, it is not possible to make correct estimations of the spherulite size in the composites based on polarized microscopy.

3.2.4. Tensile Properties

The influence of the glass sphere size and the T_{Ch} on the weld strength between adjacent strands is summarized for the 90°-oriented tensile test specimens in Figure 8. The detailed σ_Y , ϵ_Y , and E_t values are reported in Table S1 (Supporting Information). The tensile test results on the printed parts can hardly be compared to those of the filaments (Figure 2e), as both show a different failure mechanism. The filaments rupture due to material failure, whereas the printed specimens fail at the weld lines. As a result, the strain at break of neat PP decreases drastically from 1631 \pm 21% for the filaments to 9.9 \pm 1.7% for the parts printed at a T_{Ch} of 25 °C (Figure 8a). Similar findings were observed for welded joints made of PP, in which the strain at break is also considerably lower for the welded material than for the bulk material.^[76] As expected from studies on the ultrasonic^[77] and vibration-weld strength for filled PP,^[68] the addition of the glass spheres E-2 and E-3 results in a significant decrease of the σ_Y (16.5 \pm 0.7 and 15.6 \pm 0.4 MPa, respectively) and in a slight decrease of the ϵ_Y (4.2 \pm 1.1% and 4.8 \pm 1.3%, respectively) compared to neat PP (18.6 \pm 0.9 MPa and 6.4 \pm 0.6%) (Figure 8b) due to the reduced polymer volume fraction at the interface. On the contrary, the composite PP/E-1 exhibits a comparable σ_Y (18.1 \pm 0.9 MPa) to neat PP, as the smaller particles can take up higher stress concentrations at their interface.^[41] However, PP/E-1 shows a significantly smaller ϵ_Y (2.5 \pm 0.4%) than the comparable PP/E-2 and PP/E-3. The reason for that unexpected trend could be the considerably higher T_{Cryst} of PP/E-1 (125.3 \pm 0.9 °C) compared to PP/E-2 (116.8 \pm 0.6 °C) and PP/E-3 (118.9 \pm 0.5 °C) (Figure 4). An increased T_{Cryst} means that during cooling, adjacent strands have less time

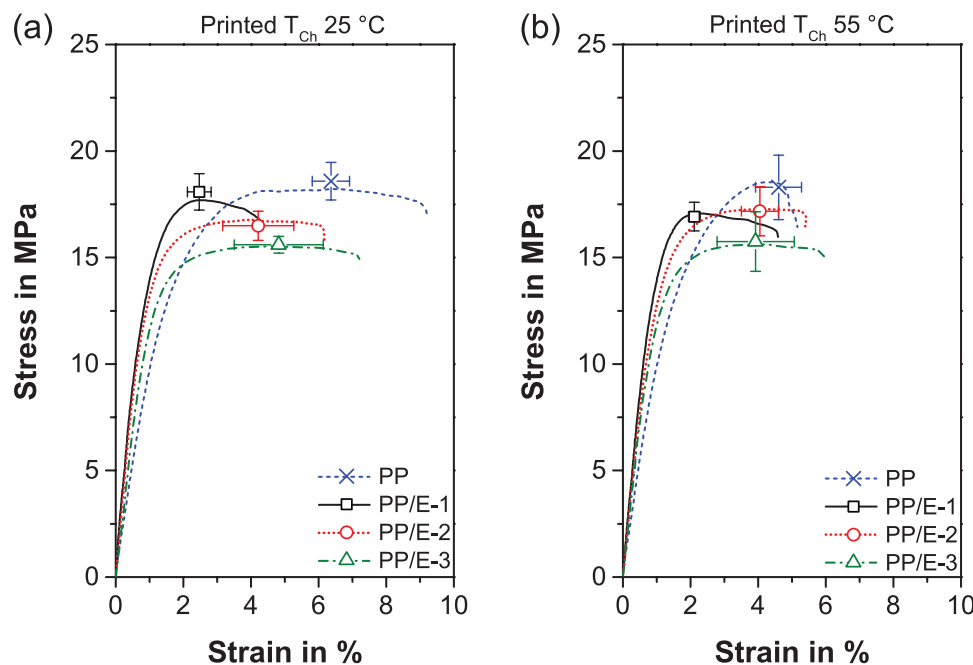


Figure 8. Representative stress–strain curves of neat PP and the three compounds investigated, measured from parts printed at a chamber temperature T_{Ch} of a) 25 °C and b) 55 °C. The mean and confidence interval for a significance level of 5% for the yield stress and the corresponding strain are marked by symbols and error bars.

to interdiffuse, as mostly amorphous chain segments are responsible for the diffusion.^[78] Hence, the material with the higher T_{Cryst} has less time to form a strong weld line,^[79–81] resulting in decreased ε_Y values.

For the higher T_{Ch} of 55 °C, elevated σ_Y and ε_Y values could be expected due to an increased interdiffusion at the strand interface in consequence of the higher temperature,^[33,78,80] similarly to the effect of increased mold temperatures in injection-molded PP weld lines.^[81] However, the investigated filled materials printed at a T_{Ch} of 55 °C (Figure 8b) do not show any significant changes in σ_Y nor in ε_Y compared to the lower T_{Ch} of 25 °C (Figure 8a). This may be related to the rapid decrease of the weld temperature^[22] to values below the T_{Cryst} of the materials, independent of the T_{Ch} (Figure 3). Hence, the time until the start of crystallization is comparably short for both T_{Ch} , resulting in unaltered mechanical properties. Most likely, improved mechanical properties can be expected, if higher T_{Ch} were used, in which the T_{mean} is above the T_{Cryst} . Nevertheless, the increased T_{Ch} strongly affects the T_{mean} (Figure 3) and therefore the growth of the spherulites (Figure 7). Consequently, neat PP printed at a T_{Ch} of 55 °C (Figure 8b) exhibits a significantly reduced ε_Y ($4.6 \pm 0.7\%$) compared to PP printed at 25 °C ($6.4 \pm 0.6\%$), as larger spherulites deteriorate the strain values.^[23,82]

To sum up, the glass spheres only slightly directly influence the property of the weld. The fillers rather affect the cooling conditions (T_{Cryst} , T_{mean}), which in turn determine the properties of the weld.

3.2.5. Impact Properties

On the contrary to the investigations of the weld line, the impact properties are directly determined by the matrix, the filler, and their interface and not by the weld lines, as the Charpy specimens are printed in a way that the strands are oriented perpendicularly to the impact direction. As expected, the incorporation of spherical fillers as well as the change in the T_{Ch} influences the impact behavior of the printed parts (Figure 9). Independent of the processing conditions, all the

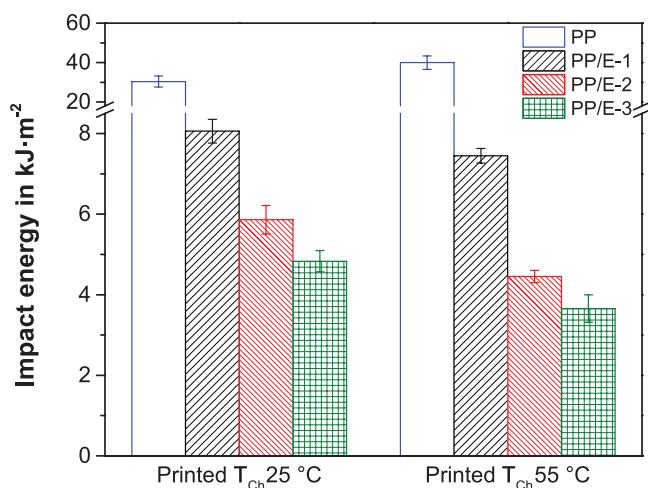


Figure 9. Impact energy for neat PP and the three compounds printed at a chamber temperature T_{Ch} of 25 and 55 °C.

composites exhibit a notched impact energy decreased by 70–90% compared to neat PP, because the incorporated microspheres can act as initiation points for defects^[20,45,83] and can reduce the impact fracture area.^[84,85] A similar decrease in the impact energy by 65% to 80% was observed for 3D-printed Charpy specimens of the same PP compound filled with the broadly distributed glass spheres Spherglass 3000E in a previous work.^[12] However, the impact energies from ref. [12] (neat PP exhibited an impact energy of $73.1 \pm 17.7 \text{ kJ m}^{-2}$) are not comparable to those of the present work (the same setting for neat PP reveals an impact energy of $40.0 \pm 3.4 \text{ kJ m}^{-2}$, Figure 9), since the latter specimens were printed at a higher flow rate. Hence, less voids and air gaps are present in the printed parts. This can decrease the amount of fracture stops, deflections, and delaminations, resulting in smaller impact areas and eventually in lower impact energies.^[12] A visualization of the reduced amount of voids is exemplarily given for the composite PP/E-2 in Figure S4a (Supporting Information).

As for all the composites, the matrix–filler adhesion after fracture is still comparable to that of the filament (Figure 2), which is exemplarily shown for the composite PP/E-2 in Figure S4b (Supporting Information), and the α_{Cryst} is comparable for all the composites, the differences in the impact results for the composites are solely related to the filler size. Similar to a study on injection-molded PP filled with inorganic soda lime glass spheres,^[20] a trend toward decreasing impact energies for increasing filler sizes is observed (Figure 9). The reason for this trend is the larger interfacial area of the smaller microspheres at a given filler content, which leads to a more frequent debonding of interfaces and therefore consumes more impact energy.^[86,87] Moreover, compared to compounds consisting of larger fillers with the same volume fraction, composites containing smaller fillers have thinner matrix ligaments that interconnect easier. Hence, the yielding process is allowed to propagate over the matrix in a more efficient way by taking up higher stress concentrations, resulting in higher impact energies.^[87,88]

An increase in the T_{Ch} to 55 °C results in the same trend for the composites as for the lower T_{Ch} . However, all the filled materials show a significant decrease (between 8% and 25%) in the impact energy compared to those printed at a T_{Ch} of 25 °C, as the larger spherulites, originating from the annealing at the T_{mean} of 84.4 °C during printing (Figure 3), decrease the amount of molecular entanglements between individual spherulites, resulting in weaker impact properties.^[89] Neat PP, however, shows an elevated impact energy for the higher T_{Ch} , although it also contains considerably larger spherulites than PP printed at 25 °C. For neat PP, this effect on the impact energy seems to be outperformed by the existence of β -crystals (Figures 5 and 6). PP containing β -crystals generally show higher impact energies than those only consisting of α -crystals,^[57,70] because the β -phase can improve the molecular entanglements between spherulites.^[90]

3.2.6. Warpage Analysis

Figure 10 summarizes the warpage results of the four investigated materials for both T_{Ch} after the removal of all the

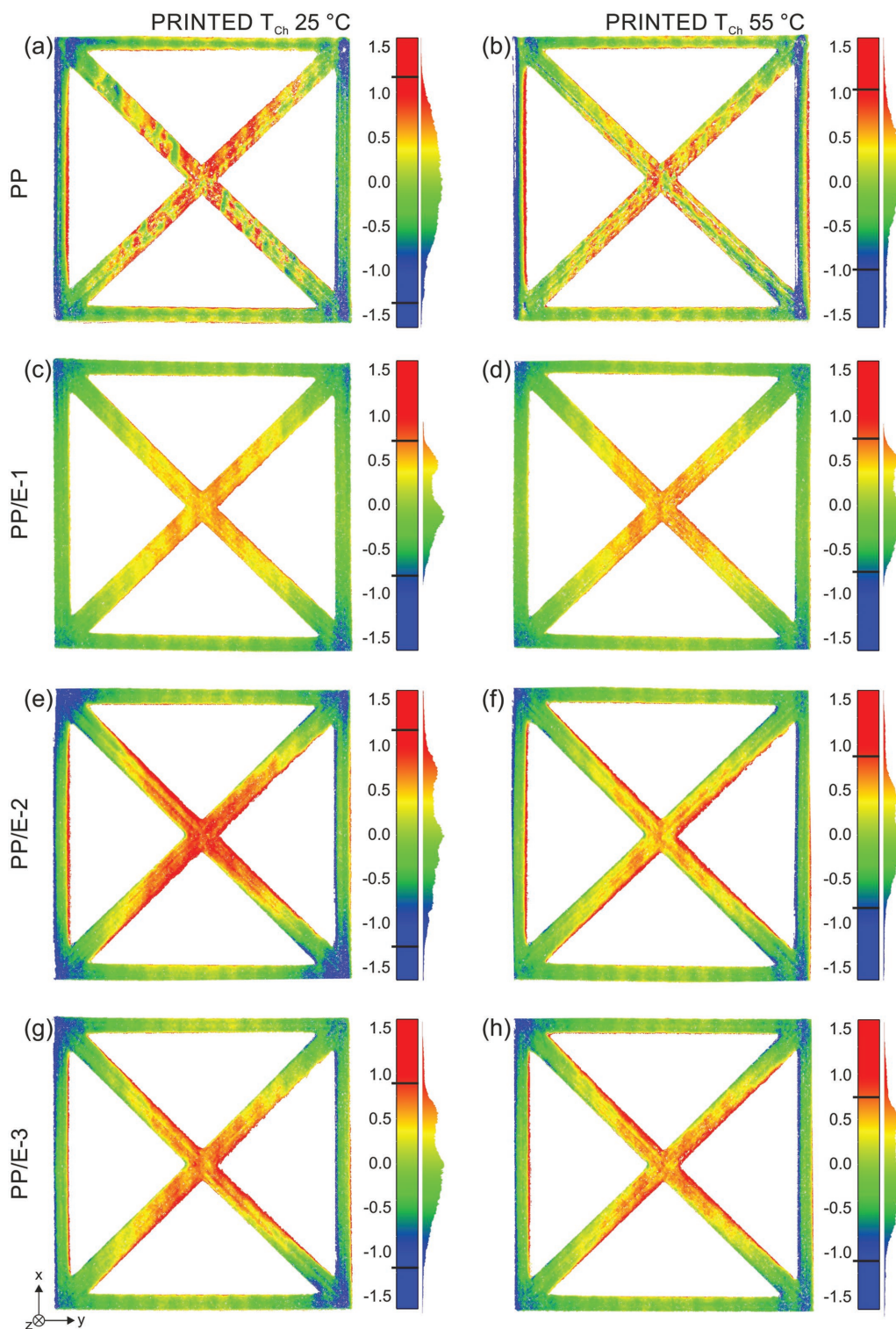


Figure 10. Results of the optical warpage analysis of a,b) neat PP, c,d) PP/E-1, e,f) PP/E-2, and g,h) PP/E-3 for the printing chamber temperatures T_{ch} of 25 °C (left side) and 55 °C (right side). All the values are deflections from the CAD geometry, given in millimeters. The coordinate system represents the part orientation based on ref. [10]. The scanned specimens are displayed in a way that the first printing layer closest to the printing bed is visible as the scanned surface. Hence, the blue area, given as negative values, reflects a warpage that is pointing away from the printing bed (in positive z-direction), whereas the red area represents a combination of shrinkage and warpage in negative z-direction. No deflection from the CAD geometry (0.0 mm), which is the ideal condition, is presented by the green area. Next to all the color codes, a histogram is given, which reflects the displacement distribution of the measured distances to the CAD geometry. The maxima and minima of the displacement distributions are labeled as black horizontal lines in the color codes.

potential surface impurities. The color code represents the distances of the printed part to the CAD geometry in millimeters that arise due to the internal/residual stresses of the material, induced by its thermal history.^[91] Ideally, no deflection from the CAD geometry (0.0 mm, green area) is present. As some warpage analyses appear similar, the intervals of the displacement distribution, marked as the black horizontal lines in the color codes, and the histograms next to the color codes give a better understanding of the warpage behavior of the printed parts. As expected, for the prints conducted at a T_{Ch} of 25 °C, neat PP suffers heavily from warpage, as can be seen from the extensively deformed corners (Figure 10a, in blue) and shrunk central parts (in red). Nevertheless, the amount of warpage is low compared to previous studies.^[10] Although compared to ref. [10] the thickness of the specimens in the present work is doubled (Section 2.12), the deflection range, which is the range between the limits of the displacement distribution, is reduced from 3.0 to 2.5 mm. This is caused by the slight differences in polarities of the PP grades of the filament and the printing bed. Hence, the first layer thickness could be decreased in the present work due to a reduced risk of welding (Section 2.5). Consequently, the adhesion increased and therefore the warpage of the printed part decreased.^[92]

The incorporation of spherical glass spheres, independent of the size, tends to minimize the warpage compared to neat PP. For the composites printed at a T_{Ch} of 25 °C, drastic differences in their warpage can be discerned (Figure 10c,e,g). As the α_{Cryst} is insignificantly different for all the composites (Table S2, Supporting Information), it is not an influencing factor for the warpage analysis.^[93] Hence, the differences in warpage for the composites can be mainly attributed to the glass sphere size. The larger fillers, especially those in PP/E-2, only show a slight improvement in warpage compared to PP, as their intervals of the displacement distribution appear similar. On the other hand, PP/E-1 (Figure 10c) reveals a strong decrease of the warpage, both in the corners and in the center of the part. Its deflection range (1.5 mm) is also considerably decreased compared to that of PP/E-3 (2.0 mm), PP/E-2 (2.4 mm), or neat PP (2.5 mm). This trend toward an improved warpage reduction for the compounds containing smaller fillers is attributed to the bigger effective interfacial area between the filler and the matrix for the smaller fillers.^[17] The observed trend is in agreement with studies on injection-molded talc^[17] and glass bead compounds^[16] and 3D-printed perlite composites.^[10] The observed good matrix–filler adhesion and the homogeneous distribution of the fillers (Figure 2) further promote an improved shrinkage and warpage.^[94] Additionally, rough changes in the height of the surface, visible especially in the center of the specimen (Figure 10a) as rapid color alterations from green to red, can be observed for neat PP. This coexistence of positive and negative deflections is due to the rougher surface quality of neat PP compared to the composites.^[10] All the composites show a much smoother surface, as no rapid color changes occur.

The specimens printed at a T_{Ch} of 55 °C show the same trend as for 25 °C. However, except for PP/E-1, the warpage of all the materials decreases with increasing T_{Ch} , as expected from the proposed mathematical model of Wang et al.^[27] As

for both T_{Ch} , the temperature differences between the printing bed and the chamber, which have a considerable effect on the part deformation,^[14] are comparably small, the warpage behavior is mostly influenced by the homogeneity of the temperature in the printing chamber and the entropy of the polymer chains. The parts printed at 25 °C are cooled down more rapidly than those printed at 55 °C, resulting in higher internal stresses^[14,26] and elevated specific volumes at room temperature. As the polymer chains attempt to decrease their specific volume to that of the infinitely slowly cooled parts^[55] during and after the fabrication process in order to reach a thermodynamically more stable state, the rapidly cooled parts shrink more over time. Higher T_{Ch} , equaling higher mold temperatures in injection molding, decrease internal stresses^[26] and entail lower specific volume differences to the infinitely slowly cooled parts at room temperature. Moreover, higher T_{Ch} allow more time for the material to crystallize completely. As a result, the long-term dimensional stability and quality improves.^[14] Furthermore, the exposure time to the increased T_{Ch} of one warpage specimen of roughly 110 min is considerably longer than typical cooling times in an injection mold. Hence, during printing, the material is annealed, which can further promote stress relaxations and crystallization processes, resulting in a part that is less prone to warpage.^[14] Only the composite PP/E-1 does not show an improvement in the warpage behavior when printed at a higher T_{Ch} (Figure 10d), as most likely the minimally achievable deformation is reached already at 25 °C (Figure 10c).

4. Conclusion

In summary, this study demonstrates the successful combination of a well-controllable warpage deformation with good mechanical properties in extrusion-based additive manufacturing of PP filled with borosilicate glass spheres. By varying the glass sphere size in the compounds, a composite containing 30 vol% of microspheres with diameters below 12 μm is proposed as the most promising material, because this composition reveals the highest filament strain at yield among the investigated composites and even higher strength values than neat PP. Furthermore, it exhibits a good filler–matrix adhesion, a homogeneous filler distribution, a 12% increase in the crystallization temperature, and a slightly reduced degree of crystallinity compared to neat PP. For the printed filled PP parts, this composite shows the highest impact strength and by far the best controllable warpage.

It was additionally found that an increase in the printing chamber temperature T_{Ch} can significantly alter the crystalline properties and, thus, all the properties of the printed parts. As for the high T_{Ch} (55 °C) the maxima of the strand temperatures surpass 100 °C, an additional β -crystal modification is found among the α -dominated PP. Moreover, for the high T_{Ch} , the mean strand temperatures during printing are roughly 84 °C over a time of 95 min. Consequently, these parts are annealed close to the temperature of the maximum crystal growth rate of PP (77 °C), resulting in twice as large spherulites as those printed at a T_{Ch} of 25 °C. Therefore, both the elongation at break and the impact energies are decreased



for the high T_{Ch} . However, the warpage of the printed parts improves compared to the low T_{Ch} , due to the more homogeneous temperature distribution within the printing chamber and the reduced amount of internal stresses at higher T_{Ch} . By keeping the spherulite size constant, e.g., through the addition of nucleating agents, and by further increasing the T_{Ch} , an optimum mechanical property portfolio could be achieved in the future.

Our findings provide two possible solutions to improve the mechanical properties, while optimizing the dimensional control of printed PP composites. When combined, crystallographic changes in the matrix material are found that can be utilized in a beneficial way to control the material properties. This study enables a deeper understanding of semicrystalline printing materials that are exposed to higher surrounding temperatures during printing and exemplifies the consequences of such process changes. Both strategies, either on their own or combined, can be applied to a wide range of semicrystalline materials for FFF and appear particularly promising for many fields of applications.

Supporting Information

Supporting Information is available from the Wiley Online Library or from the author.

Acknowledgements

This work was supported by the Austrian Research Promotion Agency (FFG) as part of the NextGen3D project (Next Generation 3D, Grant Agreement 848624). Special thanks go to Chethan Savandaiah for the assistance in filament extrusion, to Anwesh Netti for the help in the warpage analysis, to Maja Kuzmanović and Davy Deduytsche for the assistance in XRD measurements, and to Petra Erdely, Dr. Janak Sapkota, and Dr. Joamin Gonzalez-Gutierrez for fruitful discussions.

Conflict of Interest

The authors declare no conflict of interest.

Keywords

additive manufacturing, glass fillers, microstructures, poly(propylene) (PP), shrinkage and warpage

Received: March 19, 2018

Revised: April 10, 2018

Published online:

[1] Austrian Standards Institute, 2017-06-01, 01.040.25; 25.030.

[2] I. Gibson, D. W. Rosen, B. Stucker, *Additive Manufacturing Technologies: 3D Printing, Rapid Prototyping, and Direct Digital Manufacturing*, 2nd ed., Springer, New York 2015.

[3] M. Spoerk, F. Arbeiter, H. Cajner, J. Sapkota, C. Holzer, *J. Appl. Polym. Sci.* 2017, 134, 45401.

- [4] A. Gebhardt, J. Kessler, L. Thurn, *3D-Drucken: Grundlagen und Anwendungen des Additive Manufacturing (AM)*, 2nd ed., Carl Hanser Verlag GmbH & Co. KG, München 2016.
- [5] M. Gurr, R. Mülhaupt, in *Comprehensive Materials Processing* (Eds: S. Hashmi, G. F. Batalha, C. J. vanTyne, B. Yilbas), Elsevier, Oxford 2014, pp. 77–99.
- [6] F. Arbeiter, M. Spoerk, J. Wiener, A. Gosch, G. Pinter, *Polym. Test.* 2018, 66, 105.
- [7] O. S. Carneiro, A. F. Silva, R. Gomes, *Mater. Des.* 2015, 83, 768.
- [8] N. Mohan, P. Senthil, S. Vinodh, N. Jayanth, *Virtual Phys. Prototyping* 2017, 12, 47.
- [9] J. L. White, D. D. Choi, *Polyolefins: Processing, Structure Development, and Properties*, Hanser, München 2005.
- [10] M. Spoerk, J. Sapkota, G. Weingrill, T. Fischinger, F. Arbeiter, C. Holzer, *Macromol. Mater. Eng.* 2017, 302, 1700143.
- [11] D. Stoof, K. Pickering, *Composites, Part B* 2018, 135, 110.
- [12] M. Spoerk, C. Savandaiah, F. Arbeiter, J. Sapkota, C. Holzer, *Polym. Compos.* 2017, 83, 768.
- [13] L. Wang, W. Gramlich, D. J. Gardner, Y. Han, M. Tajvidi, *J. Compos. Sci.* 2018, 2, 7.
- [14] J. M. Fischer, *Mold Shrinkage and Warpage Handbook*, Plastics Design Library/William Andrew, Inc., Norwich, NY 2002.
- [15] M. Spoerk, C. Savandaiah, F. Arbeiter, S. Schuschnigg, C. Holzer, *ANTEC Anaheim*, Anaheim, CA, USA, Society of Plastics Engineers, 2017.
- [16] J. G. Kovács, B. Solymossy, *Polym. Eng. Sci.* 2009, 49, 2218.
- [17] M. W. Kim, S. H. Lee, J. R. Youn, *Polym. Compos.* 2010, 31, 1020.
- [18] J. Z. Liang, R. K. Y. Li, *Polym. Compos.* 1998, 19, 698.
- [19] B. A. Sjögren, L. A. Berglund, *Polym. Compos.* 1997, 18, 1.
- [20] K. W. Kwok, Z. M. Gao, C. L. Choy, X. G. Zhu, *Polym. Compos.* 2003, 24, 53.
- [21] S. F. Costa, F. M. Duarte, J. A. Covas, *J. Mater. Process. Technol.* 2017, 245, 167.
- [22] J. E. Seppala, K. D. Migler, *Addit. Manuf.* 2016, 12, 71.
- [23] G. W. Ehrenstein, *Polymer Werkstoffe: Struktur – Eigenschaften – Anwendung*, 3rd ed., Carl Hanser Verlag GmbH & Co. KG, München 2011.
- [24] W. Zhong, F. Li, Z. Zhang, L. Song, Z. Li, *Mater. Sci. Eng., A* 2001, 301, 125.
- [25] Q. Sun, G. M. Rizvi, C. T. Bellehumeur, P. Gu, *Rapid Prototyping J.* 2008, 14, 72.
- [26] J. Zhang, X. Z. Wang, W. W. Yu, Y. H. Deng, *Mater. Des.* 2017, 130, 59.
- [27] T.-M. Wang, J.-T. Xi, Y. Jin, *Int. J. Adv. Manuf. Technol.* 2007, 33, 1087.
- [28] W. O'kane, R. Young, A. Ryan, *J. Macromol. Sci., Part B: Phys.* 1995, 34, 427.
- [29] L. Poussin, Y. A. Bertin, J. Parisot, C. Brassy, *Polymer* 1998, 39, 4261.
- [30] D. Ferrer-Balas, M. Maspocho, A. B. Martinez, O. O. Santana, *Polymer* 2001, 42, 1697.
- [31] L. Wang, D. J. Gardner, *Polymer* 2017, 113, 74.
- [32] L. Wang, W. M. Gramlich, D. J. Gardner, *Polymer* 2017, 114, 242.
- [33] B. V. Reddy, N. V. Reddy, A. Ghosh, *Virtual Phys. Prototyping* 2007, 2, 51.
- [34] H. Schubert, *Chem. Ing. Tech.* 1979, 51, 266.
- [35] D. K. Owens, R. C. Wendt, *J. Appl. Polym. Sci.* 1969, 13, 1741.
- [36] E. Vidović, F. Faraguna, A. Jukić, *J. Therm. Anal. Calorim.* 2016, 127, 371.
- [37] D. W. van Krevelen, *Properties of Polymers*, Elsevier, Amsterdam 1997.
- [38] J. Z. Liang, R. K. Y. Li, *Polym. Int.* 2000, 49, 170.
- [39] L. Sobczak, O. Brüggemann, R. F. Putz, *J. Appl. Polym. Sci.* 2013, 127, 1.
- [40] R. Nasrin, A. H. Bhuiyan, M. A. Gafur, *Int. J. Compos. Mater.* 2015, 5, 155.

- [41] G. Landon, G. Lewis, G. F. Boden, *J. Mater. Sci.* **1977**, *12*, 1605.
- [42] L. A. Fasce, V. Pettarin, C. Marano, M. Rink, P. M. Frontini, *Polym. Eng. Sci.* **2008**, *48*, 1414.
- [43] I. Fisher, A. Siegmann, *Polym. Compos.* **2002**, *23*, 34.
- [44] D. Drummer, S. Cifuentes-Cuellar, D. Rietzel, *Rapid Prototyping J.* **2012**, *18*, 500.
- [45] F. Stricker, M. Bruch, R. Mülhaupt, *Polymer* **1997**, *38*, 5347.
- [46] O. Balkan, A. Ezdesir, H. Demirer, *Polym. Compos.* **2010**, *51*, 1265.
- [47] Q. Yuan, W. Jiang, L. An, R. K. Y. Li, *J. Polym. Sci., Part B: Polym. Phys.* **2005**, *43*, 306.
- [48] M. H. Alaei, P. Mahajan, M. Brieu, D. Kondo, S. J. A. Rizvi, S. Kumar, N. Bhatnagar, *Iran. Polym. J.* **2013**, *22*, 853.
- [49] P. R. Hornsby, K. Premphet, *J. Appl. Polym. Sci.* **1998**, *70*, 587.
- [50] H. S. Ha, J. Y. Woo, W. H. Kim, H. S. Kim, B. K. Kim, *Polym. Adv. Technol.* **2008**, *19*, 47.
- [51] K. Premphet, P. Horanont, *J. Appl. Polym. Sci.* **2000**, *76*, 1929.
- [52] S. Pimbert, *Int. Polym. Process.* **2004**, *19*, 27.
- [53] M. G. Huson, W. J. McGill, *J. Polym. Sci., Part A: Polym. Chem.* **1984**, *22*, 3571.
- [54] H. Quan, Z.-M. Li, M.-B. Yang, R. Huang, *Compos. Sci. Technol.* **2005**, *65*, 999.
- [55] G. W. Ehrenstein, G. Riedel, P. Trawiel, *Thermal Analysis of Plastics: Theory and Practice*, Hanser, München **2004**.
- [56] J. Li, H. Zhou, F. Xu, S. Jiang, W. Zheng, *Polym. Adv. Technol.* **2015**, *26*, 1312.
- [57] J. Varga, *J. Macromol. Sci., Part B: Phys.* **2002**, *41*, 1121.
- [58] H. Bai, Y. Wang, Z. Zhang, L. Han, Y. Li, L. Liu, Z. Zhou, Y. Men, *Macromolecules* **2009**, *42*, 6647.
- [59] Q. Yuan, W. Jiang, L. An, R. Misra, *Mater. Sci. Eng., A* **2006**, *415*, 297.
- [60] Y. Fujiwara, *Colloid Polym. Sci.* **1975**, *253*, 273.
- [61] Q. Liu, X. Sun, H. Li, S. Yan, *Polymer* **2013**, *54*, 4404.
- [62] R. H. Somani, B. S. Hsiao, A. Nogales, *Macromolecules* **2001**, *34*, 5902.
- [63] D. G. Papageorgiou, K. Chrissafis, D. N. Bikiaris, *Polym. Rev.* **2015**, *55*, 596.
- [64] M. Spoerk, J. Gonzalez-Gutierrez, C. Kukla, S. Schuschnigg, C. Holzer, in *PPS 2016 Asia/Australia Conf.* Chengdu, China, Polymer Processing Society (Ed: Q. Wang), **2016**, 10.
- [65] M. Spoerk, C. Savandaiah, F. Arbeiter, G. Traxler, L. Cardon, C. Holzer, J. Sapkota, *Composites, Part A* **2018**, unpublished.
- [66] K. Cho, D. Saheb, J. Choi, H. Yang, *Polymer* **2002**, *43*, 1407.
- [67] L. Spieß, G. Teichert, R. Schwarzer, H. Behnken, C. Genzel, *Moderne Röntgenbeugung*, 2nd ed., Vieweg+Teubner, Wiesbaden **2009**.
- [68] L. Lin, A. K. Schlarb, *Polym. Eng. Sci.* **2015**, *55*, 243.
- [69] F. Luo, K. Wang, N. Ning, C. Geng, H. Deng, F. Chen, Q. Fu, Y. Qian, D. Zheng, *Polym. Adv. Technol.* **2011**, *22*, 2044.
- [70] F. Luo, J. Wang, H. Bai, K. Wang, H. Deng, Q. Zhang, F. Chen, Q. Fu, B. Na, *Mater. Sci. Eng., A* **2011**, *528*, 7052.
- [71] Q. Dou, J. Duan, *Polym. Compos.* **2016**, *37*, 2121.
- [72] A. T. Lorenzo, M. L. Arnal, J. J. Sánchez, A. J. Müller, *J. Polym. Sci., Part B: Polym. Phys.* **2006**, *44*, 1738.
- [73] S. Damodaran, T. Schuster, K. Rode, A. Sanoria, R. Brüll, N. Stöhr, *Polymer* **2015**, *60*, 125.
- [74] T. Le Truong, Å. Larsen, B. Holme, F. K. Hansen, J. Roots, *Polymer* **2011**, *52*, 1116.
- [75] M.-R. Meng, Q. Dou, *J. Macromol. Sci., Part B: Phys.* **2009**, *48*, 213.
- [76] L. Fasce, A. Cisilino, P. Frontini, B. Marcisz, T. Czigan, *Polym. Eng. Sci.* **2007**, *47*, 1062.
- [77] E. Sancaktar, E. Walker, *J. Appl. Polym. Sci.* **2004**, *94*, 1986.
- [78] E. Jabbari, N. A. Peppas, *J. Macromol. Sci., Polym. Rev.* **1994**, *34*, 205.
- [79] B. Huang, S. Singamneni, *Proc. Inst. Mech. Eng., Part B* **2014**, *228*, 111.
- [80] C. Bellehumeur, L. Li, Q. Sun, P. Gu, *J. Manuf. Process.* **2004**, *6*, 170.
- [81] S. C. Malguarnera, A. I. Manisali, D. C. Riggs, *Polym. Eng. Sci.* **1981**, *21*, 1149.
- [82] H. Bai, F. Luo, T. Zhou, H. Deng, K. Wang, Q. Fu, *Polymer* **2011**, *52*, 2351.
- [83] O. Balkan, H. Demirer, *Polym. Compos.* **2010**, *77*, 1285.
- [84] M. Bramuzzo, A. Savadori, D. Bacci, *Polym. Compos.* **1985**, *6*, 1.
- [85] S.-Y. Fu, B. Lauke, *Composites, Part A* **1998**, *29*, 631.
- [86] S. Hikasa, K. Nagata, Y. Nakamura, *J. Adhes. Sci. Technol.* **2012**, *25*, 2615.
- [87] Q. Fu, G. Wang, *Polym. Int.* **1993**, *30*, 309.
- [88] J.-Z. Liang, *J. Appl. Polym. Sci.* **2002**, *83*, 1547.
- [89] T. Xu, J. Yu, Z. Jin, *Mater. Des.* **2001**, *22*, 27.
- [90] C. Y. Kim, Y. C. Kim, S. C. Kim, *Polym. Eng. Sci.* **1993**, *33*, 1445.
- [91] C. Casavola, A. Cazzato, V. Moramarco, G. Pappalettera, *Polym. Test.* **2017**, *58*, 249.
- [92] M. Spoerk, J. Gonzalez-Gutierrez, J. Sapkota, S. Schuschnigg, C. Holzer, *Plast., Rubber Compos.* **2018**, *47*, 17.
- [93] T. Glomsaker, E. L. Hinrichsen, Å. Larsen, P. Doshev, E. Ommundsen, *Polym. Eng. Sci.* **2009**, *49*, 523.
- [94] A. M. Cadena-Perez, I. Yañez-Flores, S. Sanchez-Valdes, O. S. Rodriguez-Fernandez, S. Fernandez-Tavizon, L. F. R. de Valle, T. Lozano-Ramirez, J. G. Martinez-Colunga, J. L. Sanchez-Cuevas, *Int. J. Mater. Form.* **2015**, *10*, 233.